Discharge studies in Micromegas detectors in a 150 GeV/c pion beam

S. Procureur[*,a], S. Aune[b], J. Ball[a], Y. Bedfer[a], M. Boyer[b], H. Colas[a,c], A. Giganon[b], P. Konczykowski[a], F. Kunne[a], C. Lahonde-Hamdoun[b], N. Makke[a], C. Marchand[a], O. Meunier[b], A. Morreale[a,d], B. Moreno[a], H. Moutarde[a], D. Neyret[a], S. Platchkov[a], F. Sabatié[a]

[a] *CEA, Centre de Saclay, Irfu/SPhN, 91191 Gif sur Yvette, France.*
[b] *CEA, Centre de Saclay, Irfu/Sedi, 91191 Gif sur Yvette, France.*
[c] *Ecole Centrale Paris, Châtenay-Malabry, France.*
[d] *National Science Foundation,Virginia 22230, USA.*

Abstract

A detailed study of several Micromegas detectors prototyped for the COMPASS and CLAS12 experiments is presented. Using a 150 GeV/c pion beam, the discharge probability was measured for several detector variants including bulk and non-bulk Micromegas. A detector equipped with an additional GEM foil as preamplification stage was also tested. A resistive coating of the readout strips was found to reduce the amplitude of the discharge by at least two orders of magnitude which was below the detection limit of the experimental setup. The effects of the micro-mesh type and material were investigated as well as the influence of the drift gap. Response in the presence of a 1.5 T transverse magnetic field was also studied. The measurements presented were performed during a RD51 beam test period.

Key words: Micro Pattern Gaseous Detectors, Micromegas, GEM, Resistive, Discharge, Spark, CLAS12, COMPASS, RD51, Geant4, simulation
PACS: 29.40.Cs, 29.40.Gx

[*] *Email address*: Sebastien.Procureur@cea.fr.

1. Introduction

The physics programme of the approved future COMPASS II experiment at CERN will measure processes with low cross sections. In order to gain statistical accuracy in these measurements, higher intensities of the incident muon and hadron beams will be employed. For tracking immediately downstream of the fixed target, it is foreseen to replace the present micro-pattern gaseous Micromegas [1, 2, 3, 4] by the next generation of these Micromegas detectors. While previously kept inactive in the center, the new Micromegas should now be equipped with central pixels to ensure the track reconstruction in the beam line. The robustness should be improved by the use of the new bulk technology [5] without a significant extra cost in the material budget.

The new detectors should cover the same area of 40×40 cm^2 and stand a hadron flux of the order of 5×10^5 mm^{-2}s^{-1}. A Geant4 simulation [6] has shown that the discharge probabilities measured with hadron beams can be quantitatively explained by very large energy deposits from highly ionizing particles. These ionizing particles originate from nuclear interactions of the incident hadrons with the detector's material. The present R&D is focused on the search of the optimal solution to decrease the impact of the discharge. This could be accomplished either by using resistive layers in order to reduce the amount of charge involved in a discharge, or by pre-amplifying the signal using a GEM foil [7]. The association of a Micromegas and a single GEM has already shown to be very promising in terms of discharge rate reduction [8]. Micromegas detectors have also been proposed to be part of the new Central Tracker of the future CLAS12 spectrometer at the Jefferson Laboratory [9]. A solution involving thin, cylindrical Micromegas using the bulk technology is currently under study. With the very high luminosity expected at CLAS12 (10^{35} cm^{-2}s^{-1}), these detectors will have to operate with several MHz of background leading to a potentially non-negligible discharge rate. The focus of the present study was to measure the discharge probability with this new generation of detectors where the micro-mesh is significantly thicker. The presence of a high transverse magnetic field with respect to the electric field in the CLAS12 environment [10] may also have a impact on the discharge occurrence. To evaluate this impact, the discharge probability was also measured with a transverse magnetic field.

In the framework of the CLAS12 and COMPASS Micromegas projects, specific studies with a high intensity hadron beam on small 10×10 cm^2 proto-

types were undertaken in order to better understand the origin of discharges. The main goals of these tests were the following:

- Study two solutions to reduce the impact of discharges in Micromegas:

  Introduce a resistive coating on the strips.

  Introduce an additional GEM foil to pre-amplify primary electrons.

- Study the discharge probability as a function of the following parameters:

  The presence of an external transverse magnetic field.

  The size of the drift gap.

  The influence of the micro-mesh and drift electrode material.

- Compare the measured discharge probabilities with the Geant4 simulation.

The performance of all detectors including spatial resolutions and efficiencies was compared and measured simultaneously with a muon beam. All the prototypes were built using identical boards and used the same gas mixture in order to minimize bias effects.

2. Experimental setup

2.1. Prototypes

The ten prototypes tested were designed at Saclay and built at CERN. The Printed Circuit Board (PCB) of all the detectors consisted of a 1.6 mm thick epoxy layer printed with 35 μm thick anode copper strips. The PCB was divided into two regions with 0.4 mm and 1 mm strip pitch and 71 strips each resulting in a 10×10 cm^2 active area. The studies documented hereafter focus on the 0.4 mm region.

The strips were connected to the AFTER [11] readout electronics with 80 cm flex cables using the two-row SMC adapters from ERNI [12].
To compare the performance of the different prototypes, two reference detectors (R3 and R4) were built using the bulk technology. These reference detectors consisted of a woven, 30 μm thick stainless steel micro-mesh, maintained at 128 μm above the anode strips by polymerized pillars covering around 3% of the active area. The drift electrode was a 23 μm aluminised Mylar foil

placed 5 mm above the micro-mesh. The remaining eight detectors differed from each other and from R3 and R4 by one parameter at a time. These parameters are summarized in Table 1. R1 was the only non-bulk detector and used a thinner micro-mesh. The detector R6 had an additional GEM foil placed 2.6 mm above the mesh with the drift gap above the GEM foil still being 5 mm thick. Detectors R7 to R10 were all resistive. R7, R8 and R9 were built on the same scheme (see Fig. 1 bottom), where anode strips were covered by a 50 μm thick insulator layer and then a resistive layer. This resistive layer was either a carbon loaded polyimide foil with a resistivity of 1 M$\Omega/\square$ (detector R7), or a layer of resistive paste with different resistivities (20 M$\Omega/\square$ for detector R8, 300 M$\Omega/\square$ for detector R9). With this resistive scheme, the signals induced by the electrons and ions were transmitted to the strips by capacitive coupling through the insulator layer. The charges are evacuated using a connection to ground on the lateral sides. Detector R10 was built differently from the previously described detectors as each strip was directly covered by 50 μm of resistive paste (see Fig. 1 up). The strips were kept insulated from their neighbors using coverlay walls between strips. The tightness of the gas volume was ensured by a 100 μm Mylar foil glued on an aluminum frame which was itself mounted on the PCB. The gas was an argon-isobutane (95%-5% in volume) mixture. The drift electric field was set to 0.5 kV/cm [1]. This value was chosen to achieve a micro-mesh transparency close to 100% and was subsequently increased to 2 kV/cm for magnetic field studies. For the R6 detector, the transfer field was set to 3.5 kV/cm.

2.2. Beam setup

The study took place in the H4 beam line at the CERN SPS during a RD51 [13] test beam period. The support structure for the detectors was installed inside the 1.5 T Goliath dipole magnet. Six prototypes were placed simultaneously every 8 cm in the beam line as shown in Fig. 2. Five of the prototypes had a vertical strip orientation (i.e. parallel to the magnetic field), while one prototype (R3) was placed horizontally to have access to the 2D beam profile. To test the ten prototypes, the following three combinations of detectors were used:

- R1, R6, R3, R2, R5, R4 (5 days of data);

[1] leading to a ratio of 60 between the electric fields in the amplification and drift regions.

Table 1: Specificity of each prototype used.

Detector	Modified Parameter with respect to R3/R4
R1	Non-bulk detector: micro-mesh:4 μm Cu grid
R2	Drift gap: 2 mm
R3	Reference
R4	Reference
R5	Drift electrode: woven, 30 μm stainless steel micro-mesh
R6	50 μm Polyimide GEM foil with a 5 μm Cu layer on each side, located 2.6 mm above the micro-mesh
R7	Resistive Kapton foil (1 M$\Omega/\square$) on 50 μm insulator layer
R8	Resistive paste (20 M$\Omega/\square$) on 50 μm insulator layer
R9	Resistive paste (300 M$\Omega/\square$) on 50 μm insulator layer
R10	Resistive paste on strips ($\sim$ 100 kΩ between point on paste surface and strip)

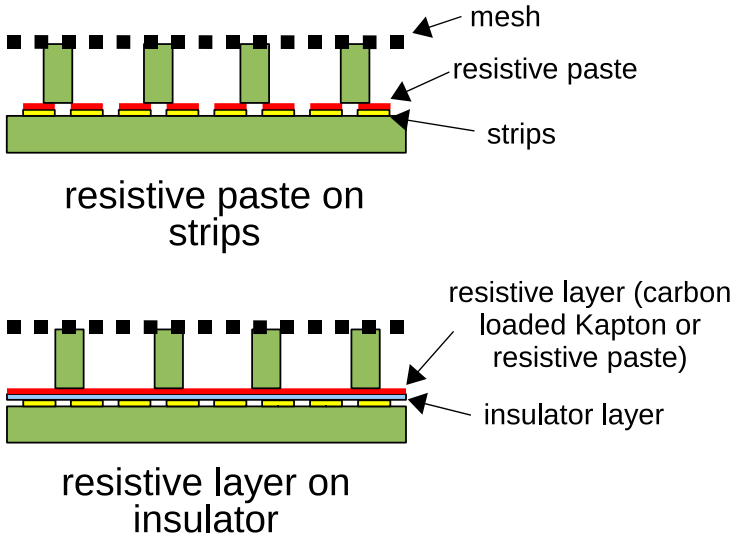

Figure 1: Scheme of R10 (up) and R7 to R9 (bottom) resistive prototypes.

- R1, R6, R3, R10, R7, R4 (2 days of data);
- R1, R6, R3, R8, R9, R4 (3 days of data).

The H4 beam line delivers 150 GeV/c pion or muon beams in spills of 10 s every 50 s. We used the low intensity (a few 10^3/spill) muon beam for perfor-

mance measurements and the high intensity (up to 10^6/spill) pion beam for the discharge rate monitoring. A coincidence between two scintillators was used as a trigger for the data acquisition. While this coincidence could also give a luminosity monitoring, we opted for the use of dedicated scintillators from the SPS beam line to access the total number of particles in each spill.

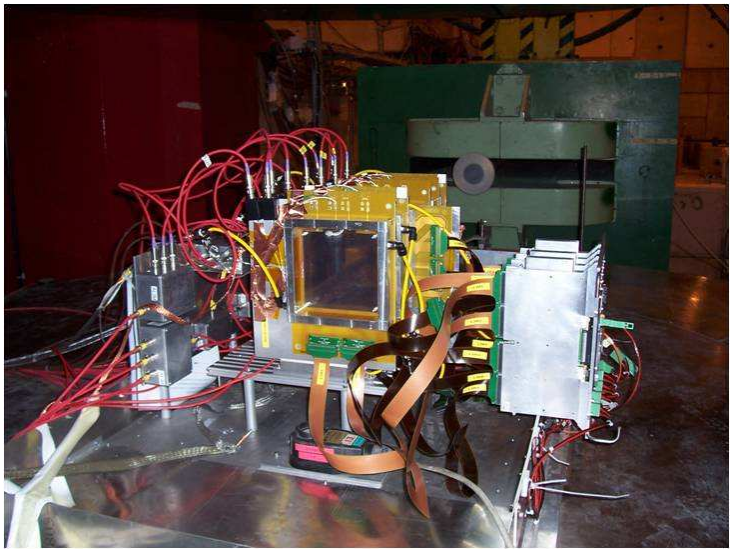

Figure 2: Six detectors in the Goliath magnet, with the readout electronics (on the right).

2.3. Discharge monitoring

A discharge in a Micromegas detector results in a rapid and abnormal increase of the micro-mesh current. This can be detected by measuring the change of the micro-mesh potential through a capacitor [2] as illustrated in Fig. 3. For the non-resistive detectors (R1 to R6), the current reaches several hundreds of nA. Using an amplifier and a discriminator with an adjusted threshold allows for an unambiguous tagging of the discharges. A CAEN V560N 16-channel VME scaler was fed with the discriminated discharge signals from the various detectors as well as a 5 Hz clock and the luminosity monitors. A CAEN V2718 VME controller was used as an interface with the DAQ computer. The DAQ controls and data taking were performed through a custom LabVIEW graphical user interface. This GUI was used to start or stop a run, display the current scaler values and write them into an ASCII

file every second to allow for offline cuts in case of detector issues or bad beam conditions.

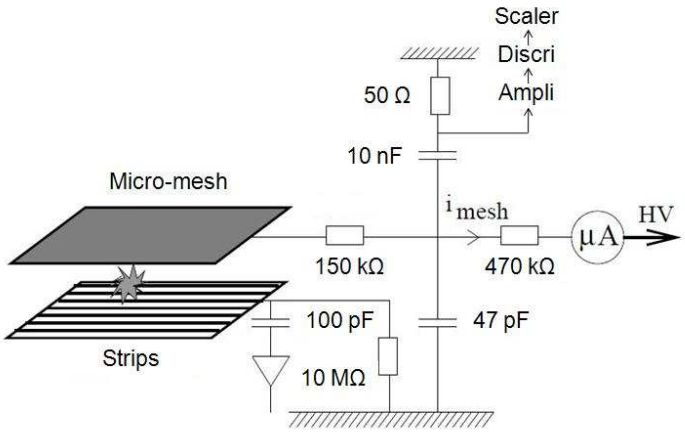

Figure 3: Schematic view of the setup used to tag the discharges, as shown in [2].

3. Gain calibration of the detectors

3.1. Principle

The gain of each detector was measured using a ^{55}Fe 5.9 keV X-ray source that provided a constant, well-defined number of primary electrons. The resulting micro-mesh signal was processed through a Multi-Channel Analyzer (MCA) used as an analog to digital converter (see Fig. 4). The position of the peak associated with the 5.9 keV X-ray is monitored in terms of MCA channels for each high voltage configuration and each detector. The conversion of MCA channels into the corresponding number of electrons N_e was obtained by injecting a known charge into the readout chain through a reference, 10 pF capacitance. The gain G was then calculated as:

$$G = \frac{N_e}{N_p}, \tag{1}$$

where N_p is the number of primary electrons generated by a 5.9 keV photon. In a 95% Ar - 5% iC_4H_{10} gas mixture, $N_p \approx 225$ [14].

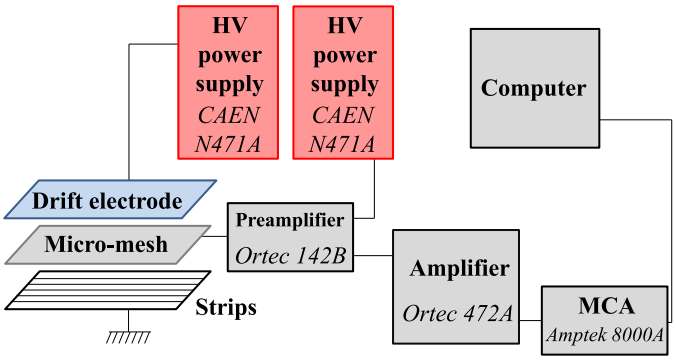

Figure 4: Schematic view of the setup used for the detector calibration.

3.2. Gain measurements

The dependence of the gain on the micro-mesh high voltage for the ten detectors is shown in Fig. 5 and 6. For resistive detectors, a decrease of the gain was observed during the first 10 to 50 minutes of source exposure. This decrease could be explained in terms of the charge up of the resistive films. The values reported here were measured once the gain was stabilized, typically after one hour of source exposure.

The gain exhibited a well-known exponential dependence as a function of the high voltage with the slopes being similar for all the detectors. For a given high voltage, gain differences of around 50% were observed for the different detector variants produced by the bulk technology. These differences could be due to small variations in the amplification gap sizes due to pressure or temperature variations during the bulk laminating process. Slightly higher maximum gains were achieved with R1 (non-bulk) compared to bulk detectors as sparks occur at smaller gains with the latter. Because of the GEM pre-amplification, R6 reached even higher gains (up to 50,000), with equal micro-mesh high voltages. Increasing the GEM voltage by steps of 20 V resulted in a relative increase of the gain by about 60% at each step.

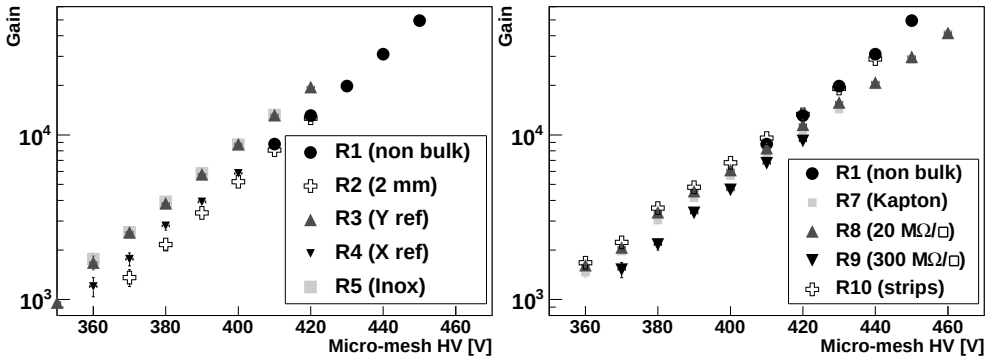

Figure 5: Gain of the bulk non-resistive (left) and resistive (right) Micromegas as a function of the micro-mesh high voltage, compared to the non-bulk Micromegas (R1).

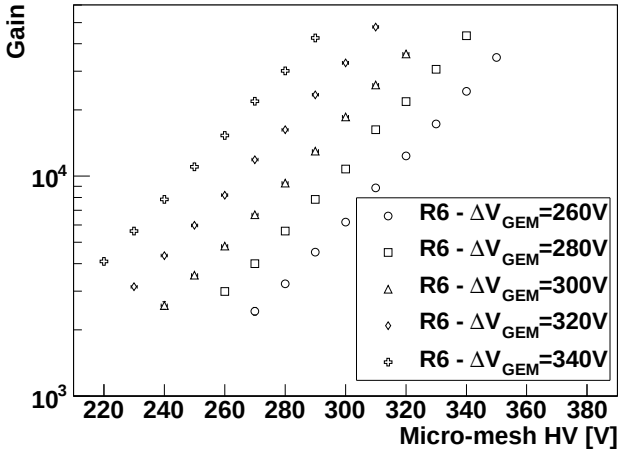

Figure 6: Gain of the R6 detector (Micromegas with GEM) as a function of the micro-mesh high voltage, and for different GEM foil voltages.

4. Results

4.1. Discharge studies versus gain, without magnetic field

Using pion beams at high intensity, the discharge probability was measured for various micro-mesh high voltages and for all the non-resistive detectors. The luminosity determined with the SPS scintillators as well as the discharge counting gave access to the discharge probability on a spill by spill

basis. Statistical studies were performed to check that this probability was stable with respect to time. The small number of discharges occurring outside the spills were discarded. No corrections were applied to compensate for the discharge dead time as it was found to be negligible even at the highest gains. The discharge rate did not exceed 1 Hz, i.e. ten per spill, while the recovery time per discharge amounted to only a few ms with the filter shown in Fig. 3. This latter observation was confirmed by the absence of an efficiency drop at the highest gains. The results for the non-resistive detectors are shown in Fig. 7. In agreement with the simulations (Section 5), no significant difference in the discharge probability between R1 and other Micromegas (Fig. 7 left) was found even though bulk detectors have much thicker micro-meshes. The simulations performed predicted a larger discharge probability for the detector equipped with a thicker drift electrode, however the dispersion of the results made the comparison difficult. Nevertheless, the R5 detector (Inox drift) gave the highest discharge probability for the four measurements at the highest gains. Finally, R4 shows systematically higher discharge probabilities compared to R3 even though these two detectors are identical. This effect could come from a dependence on the detectors position along the beam and is confirmed by the simulation (see Section 5).

Compared to detectors R1 to R5, the discharge probability of R6 (equipped with a GEM foil) is found to be smaller by about an order of magnitude (Fig. 7 right). The discharge probability is further decreased when increasing the GEM high voltage at fixed total gain. This suggests that many discharges originate from large energy deposits occurring in the transfer gap. These discharges are therefore suppressed by a reduction of the Micromegas gain. Systematic studies are under progress to better understand the role of the transverse diffusion and to check that the fraction of discharges occurring from energy deposits in the drift gap is small.

In the case of resistive detectors, discharge induced micro-mesh currents were found to be at least 100 times smaller than in non-resistive detectors and thus strongly reducing the impact of potential discharges. The equipment used during these tests for spark detection was not able to detect such small amounts of charge, therefore no discharge rate measurement for resistive detectors can be reported.

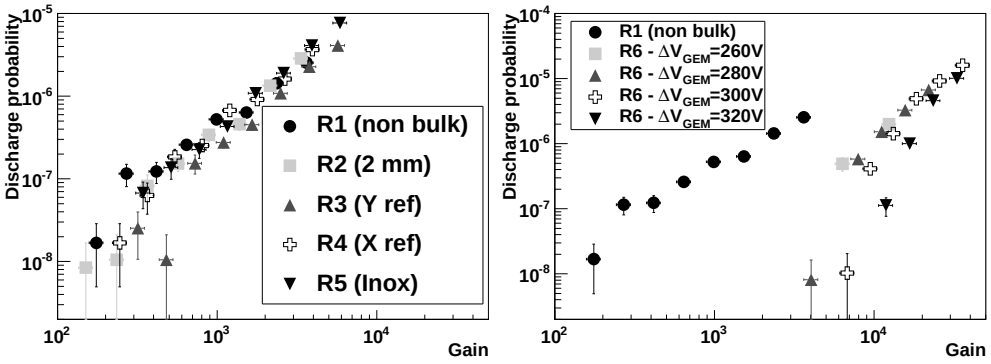

Figure 7: Discharge probability per incident hadron for bulk (left) and for R6 detector (right) as a function of their gain, compared to the non-bulk Micromegas (R1).

4.2. Effect of a transverse magnetic field

In CLAS12, part of the detectors will operate in a 5 T magnetic field perpendicular to the electric fields, leading to a Lorentz angle around 20° [10] for primary electrons. For a localized energy deposit, this corresponds to a 15% decrease of the charge density which could slightly reduce the discharge probability. With the 1.5 T field of the Goliath dipole, a similar Lorentz angle was obtained by increasing the electric field to 2 kV/cm in the conversion gap. In this configuration the micro-mesh transparency drops to 70%, and translates to a negligible efficiency loss. The discharge rate measured for different values of the magnetic field is shown for some of the detectors in Fig. 8 [2]. In spite of the small decrease of the charge density, no significant dependence of the discharge probability is observed with B.

4.3. Performance

The cluster size, spatial resolution and efficiency of all prototypes were measured with the 150 GeV/c muon beam. The dipole magnet was kept off thus providing almost straight tracks as muons had little interaction with the dead material of the detectors.

Efficiencies and spatial resolutions could be determined using a reference track from a subset of detectors as all but one detectors were oriented in the same vertical direction.

[2] these measurements were done at fixed micro-mesh high voltage, and it has been checked with the signal amplitude that the gain does not change with B.

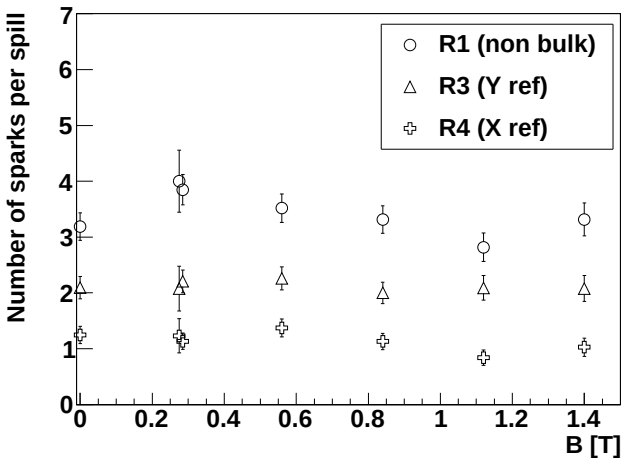

Figure 8: Discharge rate per spill as a function of the transverse magnetic field, for drift electric fields around 2 kV/cm. The micro-mesh high voltages have been set to 380 V for all three detectors, so the gains are not identical.

Detector hits created by the muon were detected and digitized by the AFTER readout system. Hits on neighboring strips were grouped together by a clustering algorithm giving access to the cluster size (i.e. the number of strips involved in the cluster). The position of the cluster was computed from the weighted average of the hits, the cluster amplitude being defined as the sum of the individual amplitudes.

A simple tracking algorithm using straight lines was applied on clusters from the detectors. The efficiency was given by the probability to find a cluster in the studied detector close to the position of the reference track and within a distance of three strips.

4.3.1. Cluster size

Mean cluster sizes are shown in Fig. 9 for the detectors with an electric field in the conversion gap of the order of 0.5 kV/cm. The sizes are given in number of 400 μm strips. Non-resistive Micromegas detectors show similar cluster sizes. Because of the transverse diffusion in the additional 2.6 mm transfer gap the cluster size for R6 is 15% larger.

For R7 to R9, the cluster sizes depend strongly on the resistance value of the layer as the spread of electrons is emphasized with small resistivities. Between 300 and 20 M$\Omega/\square$ the spread is rather limited and only visible for

gains above 4,000. The effect is much more pronounced between 20 and 1 MΩ/□, where a 50% increase is observed in the cluster size.

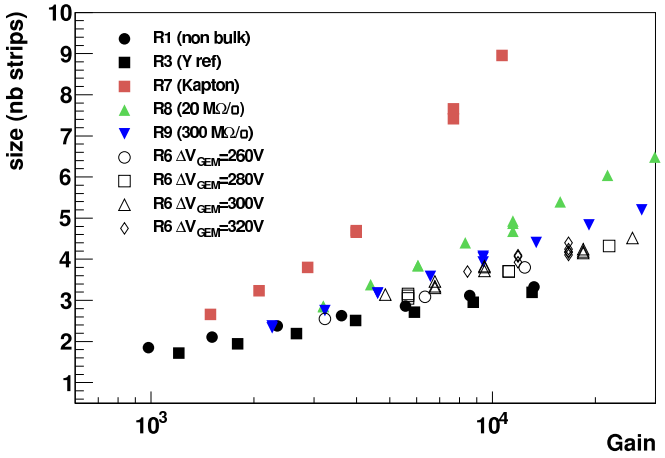

Figure 9: Mean cluster sizes measured with a low intensity muon beam.

4.3.2. Spatial resolution

Spatial resolutions were computed from residual measurements between the position of the cluster and of the reference track and properly corrected for the track resolution. For most detectors the spatial resolution was close to 70-80 μm [3] as illustrated in Fig. 10. This was significantly better than the geometrical resolution, i.e. pitch/$\sqrt{12}$. Because of the smaller transverse diffusion, the resolution is deteriorated in the case of a smaller drift gap (R2). For resistive detectors, only the prototype with the lowest resistivity (R7) had poor resolution resulting from the very large spread of electrons. As a conclusion, neither the resistive films (with high enough resistivity) nor the addition of a GEM foil degraded the resolution.

4.3.3. Efficiency

The efficiencies were also measured using a low intensity muon beam and are illustrated for some of the detectors in Fig. 11 as a function of their

[3] corresponding to residuals of the order of 110 μm

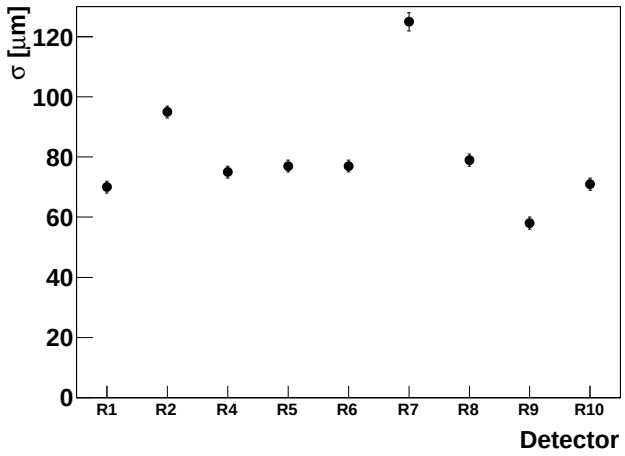

Figure 10: Spatial resolutions measured with a low intensity muon beam (G=8,000).

gain. All detectors reached an efficiency of 99%, the plateau being reached at different values. For the R2 detector (2 mm drift gap, not shown in the figure), the number of primary electrons was 2.5 times lower and thus a higher gain was needed. Resistive detectors also required a higher gain due to the spread of the charge. Measurements with the R6 prototype (Micromegas with GEM) were not performed at a low enough gain to precisely determine the beginning of the plateau.

5. Comparison with the simulated discharge probability

One of the goals of the present tests was to compare the discharge probabilities measured for the non-resistive detectors with a Geant4 simulation, where discharges are assumed to come from localized large energy deposits [6]. Using a Raether limit of 2×10^7 electrons, the simulation successfully compared with measurements performed in a 15 GeV/c pion beam [2].

Figure 12 compares the discharge probabilities measured for detectors R1 to R5 and obtained in the simulation using a Raether limit of 2.5×10^7 electrons (adjusted to better fit the data, with an error bar of 0.5×10^7). A reasonably good agreement was found for all detectors. While very different beam energies were employed, data at 15 and 150 GeV/c are well described

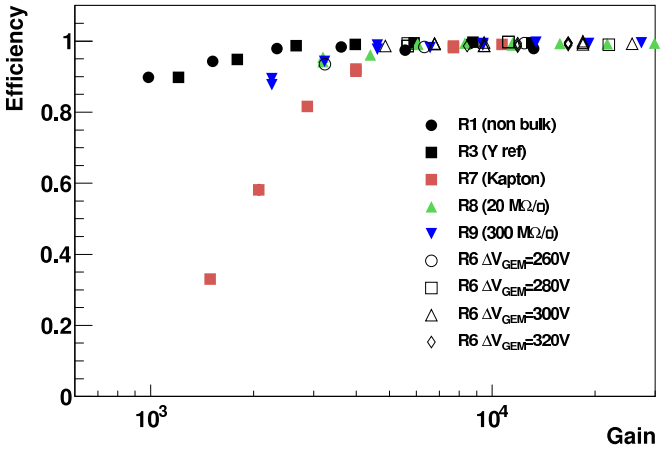

Figure 11: Efficiencies vs gain measured with a low intensity muon beam, with a drift electric field of around 0.5 kV/cm.

using an almost identical Raether limit in the simulation. For detector R5 however, it appears that too many energy deposits occur close to the thicker drift electrode and the simulation slightly overestimates the data. It is likely that a more careful treatment of the transverse diffusion in the simulation would reduce the effect of the thick drift electrode.

An interesting result of the simulation shows that for identical detectors the spark probability is slightly higher for the detectors located at the end of the experimental setup [4]. This comes from the production of secondary, low energy particles in the first detectors inducing sparks in the following detectors. The same trend was observed in the data and may explain the dispersion of the spark probabilities at a given gain.

6. Conclusion

The discharge probability was measured in a 150 GeV/c pion beam for various types of Micromegas prototypes. No significant dependence on the detector material has been observed, in particular between bulk and non-bulk detectors. For detectors R1 to R5 the simulation gives a good estimate

[4]The simulated detectors were placed along the beam line in the same order as for the data, i.e. R1/R6/R3/R2/R5/R4.

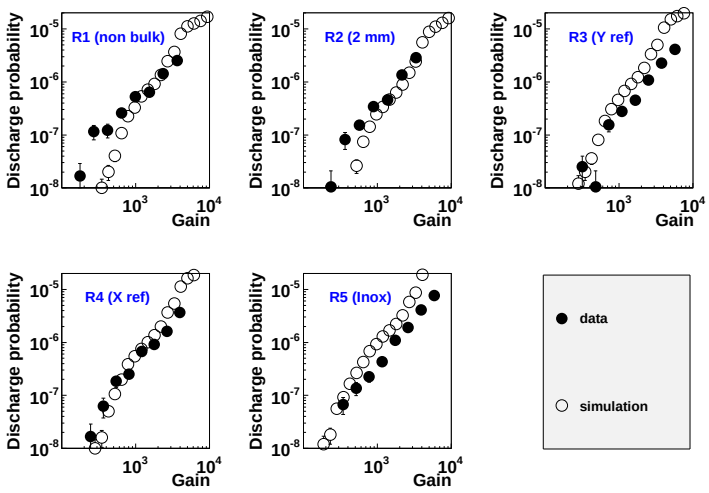

Figure 12: Comparison of the measured and simulated discharge probability for detectors R1 to R5.

of the discharge probability. Adding a GEM foil to the Micromegas reduces the discharge rate by a factor of more than 10 and suggests that most of the discharges originate from the transfer gap. Using a resistive coating suppresses the amplitude of the discharges by at least two orders of magnitude and therefore reduces their impact in terms of HV breakdowns and dead time. More careful studies are needed to further quantify the dead time reduction and to understand the charge up of the films. Aging studies are also needed before such detectors could be used in high flux experiments.

7. Acknowledgments

We are grateful to M. Alfonsi and to the RD51 staff for their help in the preparation and organization of the tests. Special thanks are also due to R. de Oliveira and the CERN/EN-ICE-DEM laboratory for the preparation of the prototypes, and to A. Magnon for useful discussions.

References

[1] I. Giomataris *et al.*, Nucl. Instrum. Methods A **376** (1996) 29

[2] D. Thers *et al.*, Nucl. Instrum. Methods A **469** (2001) 133

[3] C. Bernet *et al.*, Nucl. Instrum. Methods A **536** (2005) 61

[4] P. Abbon *et al.*, Nucl. Instrum. Methods A **577** (2007) 455

[5] Y. Giomataris *et al.*, Nucl. Instrum. Methods A **560** (2006) 405

[6] S. Procureur *et al.*, Nucl. Instrum. Methods A **621** (2010) 177

[7] F. Sauli *et al.*, Nucl. Instrum. Methods A **386** (1997) 531

[8] S. Kane *et al.*, Proceedings of the 7th International Conference on Advanced Technology and Particle Physics, Como, Italy (2001)

[9] S. Aune *et al.*, Nucl. Instrum. Methods A **604** (2009) 53

[10] P. Konczykowski *et al.*, Nucl. Instrum. Methods A **612** (2010) 274

[11] P. Baron *et al.*, AFTER, an ASIC for the readout of the large T2K time projection chambers, published in IEEE Trans.Nucl.Sci.55:1744-1752, 2008

[12] http://www.erni.com/smcfront.htd

[13] RD51 collaboration, http://rd51-public.web.cern.ch/RD51-Public/

[14] A. Sharma, SLAC-JOURNAL-ICFA-16-3